

Supplementary Information

Direct Spectroscopic Evidence of Ultrafast Electron Transfer from a Low Band Gap Polymer to CdSe Quantum Dots in Hybrid Photovoltaic Thin Films

Elsa Couderc, Matthew J. Greaney, Richard L. Brutchey and Stephen E. Bradforth**

Department of Chemistry and the Center for Energy Nanoscience, University of Southern California, Los Angeles, CA 90089, USA

Preparation of hybrid thin films

Patterned ITO-coated glass substrates ($10 \Omega \text{ cm}^{-2}$, Thin Film Devices, Inc.) were sequentially cleaned by sonication in tetrachloroethylene, acetone, and isopropyl alcohol followed by 30 min of UV-ozone treatment. A layer of PEDOT:PSS (Clevios PH 500, filtered through a $0.45 \mu\text{m}$ PTFE syringe filter) was spun-cast onto the cleaned ITO and heated at $120 \text{ }^\circ\text{C}$ for 30 min under vacuum (0.01 mmHg). Solutions of 15 mg mL^{-1} PCPDTBT were prepared in dichlorobenzene, and were mixed with dichlorobenzene dispersions of CdSe to final concentrations of 22.5 mg mL^{-1} (2.5 mg mL^{-1} PCPDTBT, 20 mg mL^{-1} CdSe), and were stirred for 2-4 h in the dark prior to use. CdSe(tBT) dispersions required 5% tetramethylurea as a co-solvent to prevent agglomeration. Active layers passed through $0.45 \mu\text{m}$ PTFE syringe filters were spun-cast in air onto annealed PEDOT:PSS layers (900 rpm, 45 s) forming films with thicknesses of $\sim 45\text{-}55 \text{ nm}$. Following spin-casting, active layer films were dried under a nitrogen

atmosphere for 20 min. ZnO nanoparticles were deposited by spin-casting to form a 20-30 nm film on top of the bulk heterojunction layer. Following the ZnO deposition, films were dried under a nitrogen atmosphere for 20 min. Dry devices were annealed at 160 °C for 10 min under nitrogen atmosphere. Finally, samples were loaded into a high vacuum ($\sim 2 \mu\text{Torr}$) thermal deposition chamber (Angstrom Engineering) for Al deposition (Al; Alfa Aesar, 99.999%) at a rate of 2 \AA s^{-1} . For spectroscopic studies, hybrid blends were deposited through a similar spin-casting procedure onto clean quartz slides (no PEDOT:PSS, ZnO, nor upper Al electrode), and encapsulated by a second quartz side glued with epoxy in a nitrogen-filled glove bag.

Steady-state optical characterization of hybrid thin films containing various QD quantities

The as-prepared hybrid thin films are studied by optical steady-state methods. The hybrid film morphology was characterized by looking at the absorbance of thin films with various QD fractions (Figure S1). The data shows a blue shift of the PCPDTBT peak absorbance with increasing CdSe(tBT) QD fraction, while maintaining a contribution to the absorbance above 800 nm. This suggests that in the hybrid films, part of the polymer chains are packed similarly to the neat polymer film, whereas another fraction of the chains is in a glassy (disordered) phase.

The legend indicates the weight and volume fraction of the CdSe(tBT) QDs in the hybrid films. The weight fractions are those used when blending the components in solution, for which the CdSe(tBT) QD weight concentrations were corrected for the ligand contributions (typically 5% for 4.5 nm tBT-exchanged CdSe QDs). The volume fractions are calculated from the weight fraction for densities of 5.8 g cm^{-3} for CdSe and 1 g cm^{-3} for PCPDTBT.

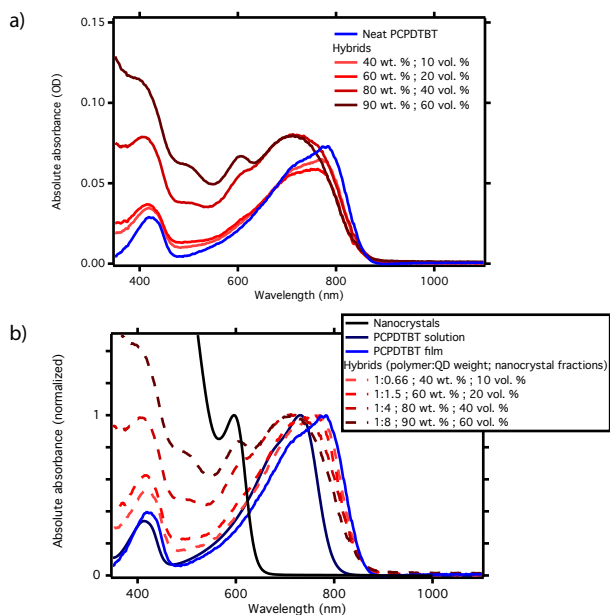


Figure S1. a) Absolute absorbance spectra of a neat PCPDTBT film and of hybrid films containing various weight fractions of QDs. b) The same, normalized to 1.0 at their reddest λ_{max} , and compared to the normalized absolute absorbance spectra of neat PCPDTBT solution and of neat CdSe(tBT) solution.

Photovoltaic device testing

The dark and one-sun illumination I - V characteristics of a photovoltaic device, whose active layer is identical to that study by TA, are given in Figure S2. Current density dependence on applied test voltage measurements were performed under ambient conditions using a Keithley 2400 SourceMeter in the dark and under ASTM G173-03 spectral mismatch corrected 1000 W m^{-2} white light illumination from an AM 1.5G filtered 300 W xenon arc lamp (Newport Oriel). The resulting device parameters were $J_{\text{SC}} = 7.25 \text{ mA cm}^{-2}$, $V_{\text{OC}} = 0.76 \text{ V}$, and fill factor of 0.38.

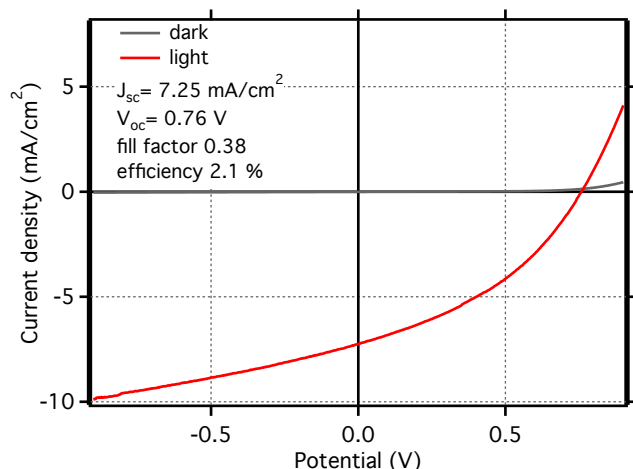


Figure S2. I - V curve for a PCPDTBT:CdSe(tBT) QD hybrid solar cell in a polymer/QD 1:8 wt/wt ratio.

Ultrafast transient absorption spectroscopy

1. *Experimental setup*

White light supercontinuum probe pulses were polarized perpendicular to the pump pulse and generated in different ways depending on the probed wavelength range. The 380-620 nm and 580-890 nm broadband continua were generated using a rotating, 2 mm thick CaF_2 window seeded with 800 nm and 1315 nm pulses respectively and detected with a Si Hamamatsu S3901-256Q photodiode array. The 850-1150 nm and 1000-1480 nm broadband continua were generated in a sapphire window, seeded with 800 nm and 1315 nm pulses respectively and detected with an InGaAs Hamamatsu G9213-256S photodiode array. The 1315 nm WL seed was generated using ca. 10% of the amplifier's output to seed a type II Spectra Physics OPA-800C. To minimize probe dispersion, a pair of off-axis aluminum parabolic mirrors was used to collimate the probe and focus it into the sample, while a CaF_2 lens focused the pump. Spectra were measured for a range of pump fluences from 30 to 2400 $\mu\text{J cm}^{-2}$, with a typical fluence of 180 $\mu\text{J cm}^{-2}$ for the 800 nm pump.

Spectra were acquired by averaging each time slice over 250 laser shots, and delay traces were scanned 5 to 10 times depending on the noise. Once acquired, data were corrected for accidental phase flips and averaged over the different time delay scans. Data obtained in different wavelength ranges were stitched together to obtain the spectra shown in the main text. In order to account for the relative absorbances of the different samples, the spectra presented in the main text are given in $\Delta A/(I_0 \times F_a)$, where ΔA is the transient absorption signal, I_0 is the incident pump photon density and F_a is the fraction of photons absorbed by a sample.

2. Transient absorption spectra of the hybrid and polymer films in mOD and normalization procedure

In the main text, we show the data normalized by the number of absorbed photons in order to account for slight variations in film thickness and morphologies. The transient absorption spectra for a neat PCPDTBT film and a PCPDTBT:CdSe(tBT) 1:8 wt/wt polymer/QDs film, presented in Figure 4 of the main text is shown here with the signal in mOD.

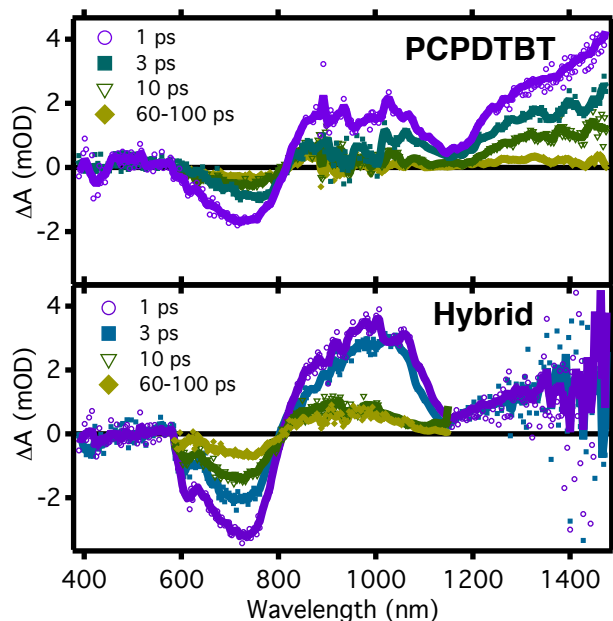


Figure S3. Transient absorption spectra of a neat PCPDTBT film (15-20 nm) and of a hybrid PCPDTBT:CdSe(tBT) film (1:8 wt/wt polymer/QDs, 45-55 nm) at different time delays between the 800 nm pump and the probe pulses. Both samples were measured with the same pump fluence and under identical conditions, but show slight differences in their absorbance. Figure 4 of the main paper shows the same data with the absorbance difference has been normalized out.

It is interesting to note that the ground state bleach amplitude is larger in the case of the hybrid than in the case of the polymer in Figure 4 of the main text. This difference does not arise from the absorbance correction, as shown in Figure S3. Both samples were measured under identical conditions. This effect likely takes its origin in the photo-induced absorption bands that overlap spectrally with the ground state bleach, modifying the shape and amplitude of the ground state bleach in different ways in the two samples. Figure S4b shows that the bleaches in the two samples exhibit slightly different shapes (for example for wavelengths above 750 nm and below 650 nm in Figure S4c and Figure S4d, as discussed in the main text and in paragraph 6 of the Supporting Information), suggesting that the overlapping photo-induced absorption bands

presumably have different amplitudes in the neat PCPDTBT film and in the hybrid film. In addition, Figure S4c and Figure S4d show that the spectral mismatches between the inverted steady-state absorption and the ground state bleach in the TA experiment are different for the neat PCPDTBT and the hybrid samples, which demonstrates different overlapping photo-induced absorption bands.

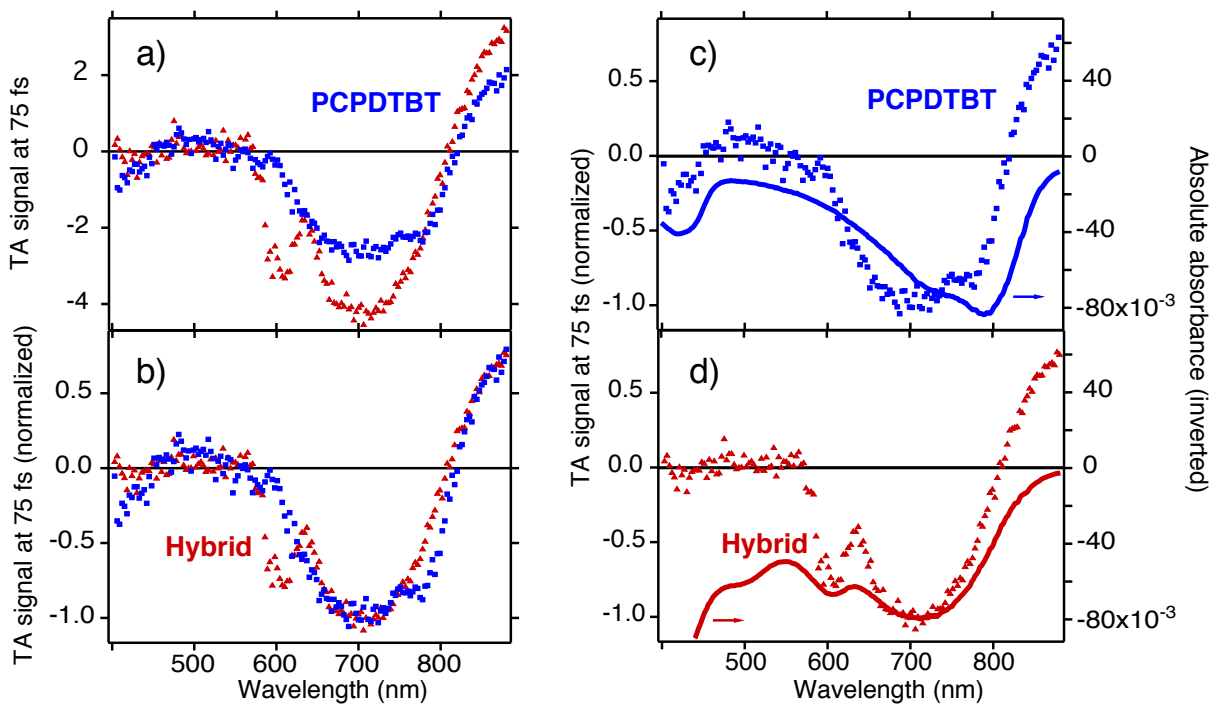


Figure S4. Comparison between the ground state bleach observed in transient absorption 75 fs after the pump pulse in the neat polymer film and in the hybrid film: the raw data in mOD is shown in (a); the normalized data is shown in (b). Comparison between the ground state bleach and the inverted steady-state absorption spectrum: in the neat PCPDTBT film (c) and in the hybrid film (d).

3. Determination of the time resolution of the transient absorption setup

The time resolution of the system, *i.e.* the pump pulse duration τ_{pump} , was found to be 65 fs based on cross-correlation between the pump and probe in two 1 mm quartz substrates (similar to encapsulated samples). The cross-correlation response was fitted to the following equation:¹

$$\Delta A(\omega_{probe}, t) \approx \exp\left(-\frac{t^2(\omega_{probe})}{\tau_{pump}^2}\right) \times \sin\left(\frac{1}{2\beta\tau_{pump}^2} - \frac{t^2(\omega_{probe})}{\beta\tau_{pump}^2} - \frac{t_0(\omega_{probe})t(\omega_{probe})}{\beta\tau_{pump}^2\tau_{probe}^2}\right)$$

where $\Delta A(\omega_{probe}, t)$ is the experimentally measured pump-induced change in optical density, ω_{probe} is the spectral component of the probe, $t(\omega_{probe})$ is the frequency-dependent pump-probe time delay, τ_{pump} and τ_{probe} are the pump and probe pulse durations, β is the chirp rate and $t_0(\omega_{probe})$ is the time-zero function, which is fitted at the peak of the cross-phase modulation signals.

4. The 900-1050 nm signal in neat PCPDTBT films likely comes from the tails of the broad exciton and polaron PIA bands

We observe a strong and long-lived PIA signal in the hybrid film, in the 900-1050 nm range (orange shading in Figure 4 and Figure 5 of the main text). A smaller PIA signal is initially present in the neat PCPDTBT films, and based on the very similar decays observed in Figure S5, we attribute the PIA in neat polymers in this wavelength region to tails of the broad PIA absorptions of the excitons and polarons.

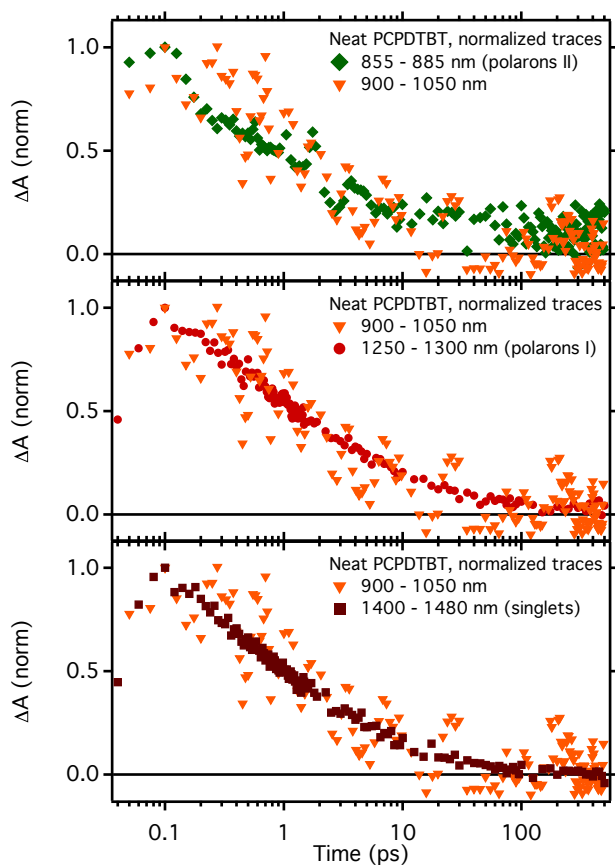


Figure S5. Transient absorption decays of the signals measured in a neat PCPDTBT film (spectra in Figure 4 of the main text).

5. Multi-exponential fits of the decays dynamics of the various excited species

The results of analysis of the decay of the excited species populations are summarized in the following table for the neat PCPDTBT and hybrid films, obtained using multi-exponential fits

$$\sum_i A_i e^{-(t-t_0)/\tau_i}.$$

Table S1. Decay dynamics of the excited species identified in the main text: multi-exponential fit parameters for the data presented in Figure 5.

Wavelength range	PCPDTBT film	PCPDTBT:CdSe QD film 1:8 wt:wt ratio
855-885 nm (attributed to PCPDTBT polarons II)	$t_1 = 0.1$ ps (6%) $t_2 = 2$ ps (60%) $t_3 = 50$ ps (18%) $t_4 > 500$ ps (16%)	$t_1 = 0.2$ ps (5%) $t_2 = 3$ ps (64%) $t_3 = 136$ ps (24%) $t_4 > 500$ ps (7%)
900-1050 nm (attributed to electrons on QD)	$t_1 = 1$ ps (68%) $t_2 = 20$ ps (32%) $t_3 > 500$ ps (0%)	$t_1 = 0.2$ ps (15%) $t_2 = 7$ ps (62%) $t_3 > 500$ ps (22%)
1250-1300nm (attributed to PCPDTBT polarons I)	$t_1 = 1$ ps (15%) $t_2 = 20$ ps (79%) $t_3 > 100$ ps (6%)	$t_1 = 0.4$ ps (19%) $t_2 = 18$ ps (61%) $t_3 > 100$ ps (20%)
1400-1480 nm ($S_n \leftarrow S_1$, attributed to PCPDTBT singlets)	$t_1 = 1$ ps (66%) $t_2 = 17$ ps (34%) $t_3 > 100$ ps (0%)	$t_1 = 0.7$ ps (25%) $t_2 = 45$ ps (73%) $t_3 > 100$ ps (2%)

6. The 500 nm region contains overlapping features including a PIA signal from PCPDTBT singlet excitons

The PCPDBT ground state bleach overlaps with a photo-induced absorption (PIA) band. The PIA band is detected as a positive contribution around 500 nm and through the deformation of the ground state bleach (the high energy polymer absorption band, located around 410 nm in the steady state absorption, is almost absent in the transient absorption spectra). Because this PIA feature is present in spectra of PCPDTBT solutions in ODCB (Figure S6), we attribute the band to high-energy singlet transitions ($S_n \leftarrow S_1$).²

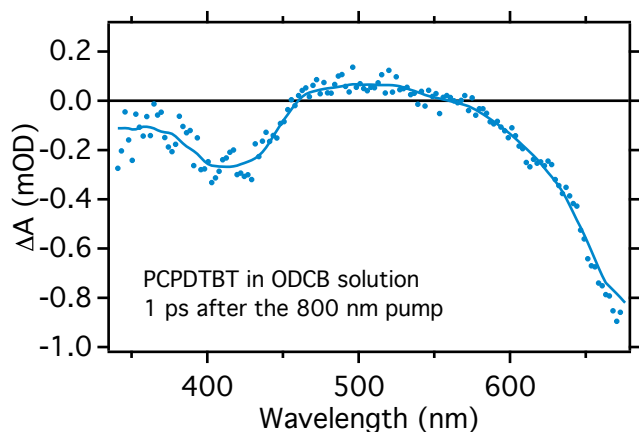


Figure S6. Transient absorption spectra of a PCPDTBT in ODCB solution at $1.6 \times 10^{-3} \text{ mg mL}^{-1}$ excited with an 800 nm pump. The pump fluence has been adjusted to get a number of absorbed photons similar to that absorbed in the films, *i.e.* $1.05 \times 10^{14} \text{ cm}^{-2}$. The data points are given as circular symbols, the full line is smoothed data.

7. Deconvoluting the spectral contributions of the polymer bleach and the QD bleach

We use Bayes' theorem to deconvolute the polymer and QD bleaches with a linear combination model.³ This approach gives access to statistically based error bars for the deconvolution process.

We used a doorway function for the prior probability density function on model parameters a and b ($0,0 < (a,b) < (10,5)$): our only a priori is that the contributions of the neat QD and neat polymer bleaches cannot be negative and cannot diverge. Because the ground state bleach of the polymer is enhanced in the hybrid relative to that in the neat film, b can be greater

than one. The likelihood is given by $\exp\left(-\frac{1}{2} \frac{(d_{\text{obs}} - d_{\text{pred}})^2}{e^2}\right)$, where e is the experimental

uncertainty and d_{obs} and d_{pred} are defined as follows:

$$d_{obs} = \frac{\Delta OD_{hybrid}}{I_0 \times F_{a,hybrid}}$$

$$d_{pred} = a \times \frac{\Delta OD_{polymer}}{I_0 \times F_{a,polymer}} + b \times \frac{\Delta OD_{QD}(t = 75 fs)}{I_0 \times F_{a,QD}}$$

The posterior probability density function is given by the product of the prior probability density function and the likelihood. A Metropolis-Hastings algorithm (Matlab Statistical Toolbox) is used to scan the parameter space (20,000 samples, 1,000 burnt samples) and obtain the most likely model parameters (a_{mean} , b_{mean}), *i.e.* the ones that maximize the posterior probability density function, as well as their standard deviations (a_{std} , b_{std}).

8. *Electron transfer yield calculation*

The parameter b of the above deconvolution gives the QD bleach contribution to the hybrid spectra. In order to backtrack this number b to the actual density of electrons on QDs, we need a “calibration” to relate the bleach amplitude to the density of electrons. For this calibration, we use the spectrum obtained from neat QD films excited directly at 550 nm, shown in Figure 4 of the main text.

We consider the amplitude of the $1S_e$ - $1S_{3/2}$ / $1S_e$ - $2S_{3/2}$ QD bleach when the neat QD film is directly excited at 550 nm. This spectrum was obtained for a density of absorbed photons $I_{0,QDs} \times F_{a,neat QD} = 5 \times 10^{14} \text{ cm}^{-2} \times 0.14 \sim 7 \times 10^{13} \text{ cm}^{-2}$. We assume that each absorbed photons results in an excited electron, part of an electron-hole pair and occupying either the $1S_e$ level or the $1P_e$ level of the conduction band of the QD. The spectrum in Figure 4 includes the bleaches of transitions involving these two electron states (*i.e.*, $1S_e$ at 610 nm and $1P_e$ at 510 nm); and we estimate the relative populations of the $1S_e$ and $1P_e$ levels from the ratio of the integrated TA bleaches at 610 nm and 510 nm – the $1P_e$ level contains $F_{1P_e} \sim 0.32$ of the electron population and

the $1S_e$ level contains $F_{1S_e} \sim 0.68$ of the electron population. Consequently, the bleach amplitude at 610 nm in the spectrum for neat QDs corresponds to a density of electrons on the $1S_e$ energy level $I_{0,QDs} \times F_{a,neat\ QD} \times F_{1S_e} = \sim 5 \times 10^{13} \text{ cm}^{-2}$.

9. The rapid decay of the electron population is due to recombination with PCPDTBT polarons

Two control experiments were carried out to support the claim that the rapid decay of the electron density in the hybrids is due to recombination with PCPDTBT polarons and not to trapping into localized states. The ground state bleach recovery of the 610 nm bleach was measured in neat QD films, with either native ligands or tBT ligands. Trapping of electrons into localized states would result in longer bleach recovery than in the absence of trapping. Here, the bleach recovery is much faster in the hybrid (ps timescale) than in both the neat QD film (ns time scale), see Figure S6, suggesting an efficient decay pathway to the ground state. In particular:

a) The dynamics of the ground state bleach of neat CdSe QD films is usually dominated by the electron relaxation due to the near degeneracy of the valence band.⁴ The ground state bleach recovery pictured in black in Figure S7 is therefore representative of the excited electron dynamics. The fact that the decay is much slower than in the hybrid shows that electrons specifically are not trapped.

b) Thiols induce hole traps at the surface of CdSe(tBT) QD. The ground state bleach recovery is greatly slowed down compared to that observed in films of CdSe capped with native ligands, as observed in the literature⁴ and in Figure S7. This slower decay is attributed to hole transfer to localized, thiol-induced excited trap states that prevent full relaxation to the ground

state and therefore ground state bleach recovery. The ground state bleach recovery pictured in red in Figure S7 is therefore representative of the dynamics of the excited, localized hole states.

c) In the PCPDTBT: CdSe(tBT) QD hybrid, the bleach at 600 nm probes only the electron dynamics in the context of the QDs, as argued in the text. The decay of the electron population in the hybrid is greatly accelerated compared to the ground state bleach in neat QD films, Figure S7. This means that the accelerated decay observed in the hybrid film is not related to localized excited states that already exist in the neat QD films. Assuming that the blending with the polymer does not induce electron traps, we therefore attribute the rapid decay of the electron density in the hybrids to recombination with the PCPDTBT polarons.

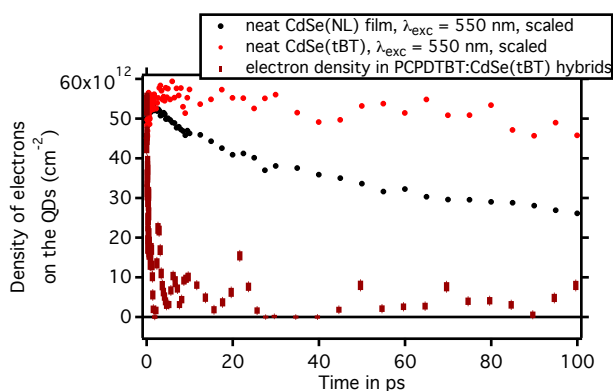


Figure S7. Time evolution of the QD electron population in the hybrid film compared to the time evolution of the 610 nm ground state bleach in the neat QD films, capped with either native ligands (black circles) and tBT (red symbols), after 550 nm excitation.

10. The rapid decay of the electron population is due to geminate recombination

In Figure S8, we show that the electron decay time does not vary with the pump fluence, confirming monomolecular recombination pathway. As for Figure 6, electron density decays were obtained from the deconvolution of the 610 nm TA bleach in two contributions, that of the

ground state bleach of the polymer and that of the bleach of the QDs. Error bars are obtained from the Bayes theorem, as described in the main text and in paragraph 7 of the Supporting Information. A solution to the electron-hole pair diffusion problem, under mutual Coulomb attraction, is shown with the black line for all fluences.

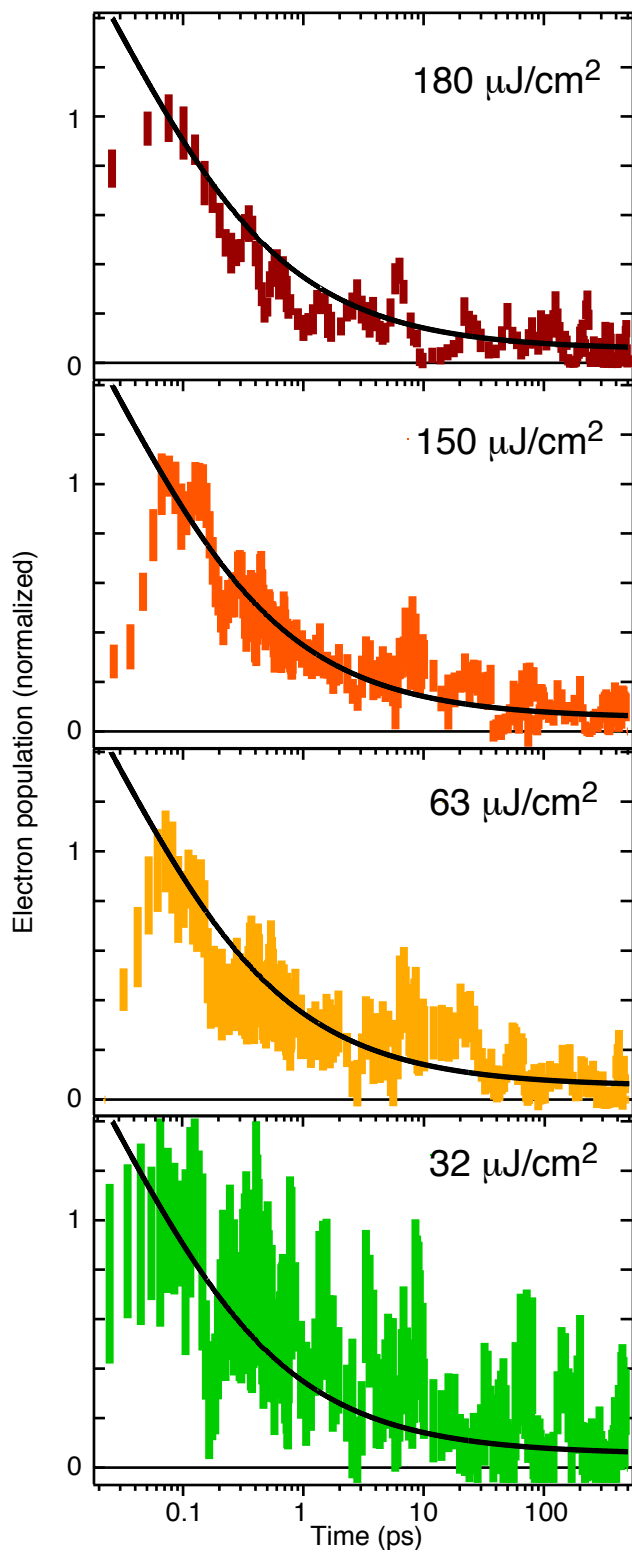


Figure S8. Normalized electron population decay as a function of time for different pump fluences. The top panel is equivalent to the data in Figure 6 of the main text; the black line is the result of our diffusion model.

11. Diffusive recombination of charge pairs under the influence of an electric field

We solve the diffusion equation describing the diffusive recombination of charge pairs under the influence of their Coulombic mutual attraction (in our TA experiments, there is no externally applied bias) with a numerical solver.⁵ In polar coordinates, the diffusion equation writes:

$$\frac{\partial \rho}{\partial t} = D \left[\frac{\partial^2 \rho}{\partial r^2} + \left(\frac{2}{r} - \frac{r_c}{r} \right) \frac{\partial \rho}{\partial r} \right] + \frac{\delta(r_0 - r) \delta(t_0 - t)}{4\pi r^2}$$

where ρ is the density of charges, r_c is the Onsager radius $r_c = \frac{e^2}{4\pi\epsilon_0\epsilon_r k_B T}$ and D is the diffusion coefficient $D = \frac{k_B T}{q} (\mu_e + \mu_h)$. Perfectly absorbing boundaries in $r = 3 \text{ \AA}$ and $r = 1000 \text{ \AA}$ limit the diffusion space. $r = 3 \text{ \AA}$ was chosen because it correspond the *tert*-butylthiol ligand length: the recombination rate is infinite (perfectly absorbing boundary) when the charges are separated by the ligand only, *i.e.* by 3 \AA . This means that we assume that recombination is diffusion limited. The initial charge pair density probability is a Gaussian distribution centered at $r = 0 \text{ \AA}$ and we varied the Gaussian characteristic length $L = \frac{\sigma}{\sqrt{2}}$ (see Figure S9a). Only the charges that are generated at $r > 3 \text{ \AA}$ are taken into account in the diffusion model (lower boundary $r = 3 \text{ \AA}$). This is a strong assumption: we hypothesize that the diffusion model accounts for all the measured charges.

The solution presented in Figure 6 of the main text (black line, also in Figure S9a) was obtained with the diffusion coefficient D calculated from measured mobility values⁶ ($\mu_e \sim \mu_h \sim 10^{-3} \text{ cm}^2 \text{ V}^{-1} \text{ s}^{-1}$) $D = 5 \times 10^{-5} \text{ cm}^2 \text{ s}^{-1}$ and the Onsager radius $r_c = 5 \text{ \AA}$ (corresponding to an effective medium dielectric constant $\epsilon_r = \frac{e^2}{4\pi\epsilon_0 k_B T r_c} \approx 112$). The pair survival probability density at various times after the generation event and the Coulomb potential are represented in Figure S8b.

Reasonable agreement with the data can also be obtained using higher Onsager radii (*i.e.* more reasonable, lower dielectric constants) together with higher initial charge separations as long as the charges are generated within r_c . On the other hand, these alternative models require high diffusion constants, up to $D = 5 \times 10^{-2} \text{ cm}^2 \text{ s}^{-1}$, *i.e.* three orders of magnitude larger than the diffusion coefficient calculated from typical measured mobility values. Two alternative models are shown in Figure S9a.

Concluding, we show that our data can be understood in a physically meaningful framework, namely that of diffusion limited recombination. While these models can explain the data, it is perfectly possible that a finite recombination rate at the interface can account for the fast population decay (<1 ps), while the diffusion of charge carriers would account for the later and slower decay (> 1 ps).

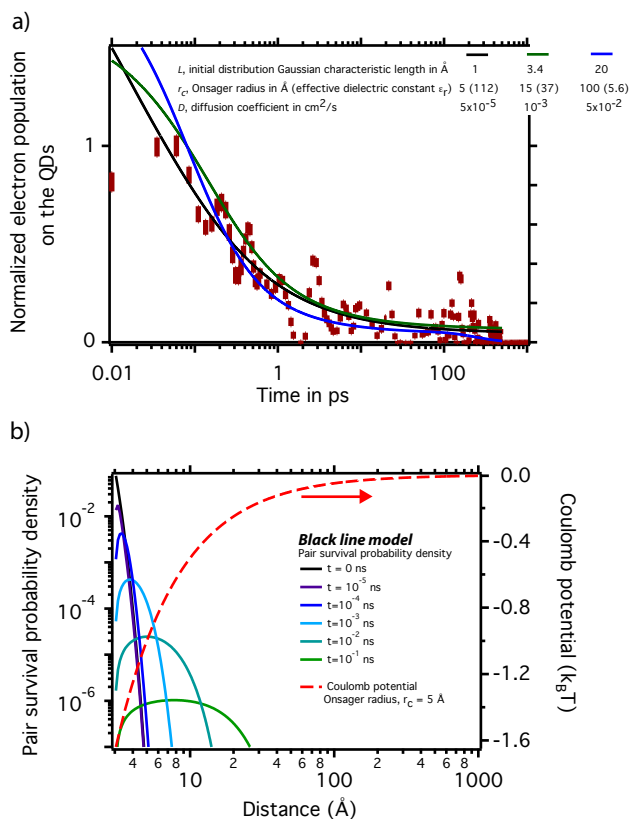


Figure S9. a) Different solutions obtained with different values of the Onsager radius r_c , initial charge separation distribution and diffusion coefficient D ; b) for the parameters used for the black line solution (main text, Figure 6, and Figure S9a), the spatial profiles of the Coulomb potential and of the pair survival probability density for various time after the generation event at time 0.

¹ Kovalenko, S. A.; Dobryakov, A. L.; Ruthmann, J.; Ernsting, N. P. *Phys. Rev. A*, **1999**, *59*, 2369-2384.

² Grancini, G.; Martino, N.; Antognazza, M. R.; Celebrano, M.; Egelhaaf, H-J.; Lanzani, G. *J. Phys. Chem. C*, **2012**, *116*, 9838-9844.

³ Press, W. H.; Teukolsky, S. A.; Vetterling, W. T.; Flannery, B. P. *Numerical Recipes in C : the Art of Scientific Computing*; Cambridge University Press, **1988**.

⁴ Burda, C.; Link, S.; Mohamed, M.; El-Sayed, M. *J. Phys. Chem. B*, **2001**, *105*, 12286-12292.

⁵ Krissinel', E. B.; Agmon, N. *J. Comput. Chem.*, **1996**, *17*, 1085–1096.

⁶ Couderc, E.; Bruyant, N.; Fiore, A.; Chandezon, F.; Djurado, D.; Reiss, R.; Faure-Vincent, J. *Appl. Phys. Lett.*, **2012**, *101*, 133301.